

1 **New archeointensity data from Novgorod (North-Western Russia) between c. 1100 and**  
2 **1700 AD. Implications for the European intensity secular variation**

3 Natalia Salnaia<sup>1</sup>, Yves Gallet<sup>2</sup>, Agnès Genevey<sup>3</sup>, Ilya Antipov<sup>4</sup>

4

5 <sup>1</sup> Institute of Physics of the Earth, Russian Academy of Sciences, Moscow, Russia,  
6 [natasavi@inbox.ru](mailto:natasavi@inbox.ru), corresponding author

7 <sup>2</sup> Institut de Physique du Globe de Paris- Sorbonne Paris Cité- Université Paris Diderot, UMR  
8 7154 CNRS, Paris, France

9 <sup>3</sup> Sorbonne Universités, UPMC Univ. Paris 6, CNRS, UMR 8220, Laboratoire d'archéologie  
10 moléculaire et structurale (LAMS), Paris, France

11 <sup>4</sup> Institute of History, St Petersburg State University, St Petersburg, Russia

12

13 **Abstract**

14 Reconstructing the secular variation of Europe's geomagnetic field over the past  
15 millennium is challenging because of the lack of recently acquired archeomagnetic data from  
16 Western Russia. In this paper, we report on nine new archeointensity values obtained from  
17 groups of brick fragments sampled in Novgorod (North-Western Russia) and its vicinities.  
18 These fragments were collected from churches whose precise ages range from the beginning  
19 of the 12th century to the end of the 17th century AD. All the archeointensity measurements  
20 were carried out using the Triaxe experimental protocol, which takes into account the  
21 thermoremanent magnetization (TRM) anisotropy effect. Intensity determinations were  
22 performed using fast and slow cooling rates for laboratory-TRM acquisition. The results  
23 confirm that the Triaxe protocol overcomes the TRM cooling rate dependence. The new data  
24 shows that geomagnetic field intensities in North-Western Russia have decreased in the past  
25 millennium. Comparisons were made with other data previously obtained in Western Europe,

26 the Balkans and Russia, as well as with intensity values expected in Novgorod from global  
27 geomagnetic field models. These comparisons yielded three main results: 1) The new  
28 archeointensity data do not show the occurrence of large intensity variations in North-  
29 Western Russia, as those observed in the Balkan dataset. Conversely, they appear more  
30 compatible with Western European results, which suggests a limited non-dipole field effect  
31 across Europe during the past millennium; 2) Our data are weaker than the intensity values  
32 expected in Novgorod from the available global geomagnetic field models. This suggests that  
33 the field models are inaccurate for the Novgorod area; 3) A constant linear decrease of the  
34 geocentric axial dipole moment since 1600 AD does not appear compatible with our younger  
35 data.

36

37 *Keywords:* Secular variation, geomagnetic field intensity, past millennium, North-Western  
38 Russia, Europe, geomagnetic field modeling.

39

40

## 41 **1. Introduction**

42 For the past 15 years, considerable efforts have been made to improve our knowledge  
43 of the secular variation in Western Eurasia's geomagnetic field over the past few millennia. In  
44 Western Europe, these efforts were focused on the recovery of both the directional (e.g. Gallet  
45 et al., 2002; Hervé et al., 2013a) and field intensity variations for the period spanning the past  
46 two to three millennia, with significant progress (e.g. Gómez-Paccard et al., 2008; 2012;  
47 2016; Gallet et al., 2009; Genevey et al., 2009; 2013; 2016; Hervé et al., 2013b; 2016).

48 The overall geomagnetic field intensity variation curve in Western Europe, which  
49 covers the past three millennia, is now one of the best documented and detailed curve  
50 worldwide. However, certain segments remain poorly constrained, suffering from an

51 insufficient number of data as is, for instance, the case for the first millennium BC (Hervé et  
52 al., 2013b; 2016). In contrast, the past 1500 years are particularly well documented, revealing  
53 a geomagnetic signal punctuated by a series of centennial-scale intensity peaks (Genevey et  
54 al., 2013; 2016). This well-defined curve demonstrates that recovering the intensity secular  
55 variation at the centennial time scale is a difficult but achievable target.

56 At present, only the important dataset obtained in the Balkans (South-Eastern Europe)  
57 including results from Bulgaria (Kovacheva et al., 2014), Greece (e.g. Tema and  
58 Kondopoulou, 2011; Tema et al., 2012) and Southern Italy (e.g. Tema et al., 2013) can be  
59 used to carry out a comparison between the geomagnetic intensity variations that occurred in  
60 Western and Eastern Europe (e.g. Genevey et al., 2013, 2016; Pavón-Carrasco et al., 2014a).  
61 The Balkan data appear rather dispersed. They exhibit large intensity fluctuations with trends  
62 like those observed in Western Europe, though with higher amplitude. The resolution of this  
63 curve, however, does not have enough detail to conclude on the occurrence of drifting non-  
64 dipole sources, westward nor eastward, between Western and Eastern Europe during the past  
65 1500 years (Genevey et al., 2016). Given the available data, Pavón-Carrasco et al. (2014a)  
66 concluded that the geomagnetic field intensity evolution over the past few millennia was  
67 likely homogeneous across Europe.

68 In other sub-regions of Europe, archeointensity data are still not numerous enough to  
69 further constrain the issue of homogeneity in intensity variations over this semi-continental  
70 wide area. This is the case for North-Western Russia, around the city of Novgorod  
71 ( $\lambda=58.52^{\circ}\text{N}$ ,  $\phi=31.27^{\circ}\text{E}$ ). Here archeointensity data dated to the Medieval period and meeting  
72 minimum quality criteria are virtually absent (e.g. Burlatskaya et al., 1986; Genevey et al.,  
73 2008; Pavón-Carrasco et al., 2014a). During the first half of the second millennium AD, this  
74 region was economically rich because of active trading with other Russian lands and the  
75 Baltic Sea countries (Rybina, 1992; 2001). Many buildings, especially churches were built at

76 that time using baked-clay bricks, which makes this region a promising target for an  
77 archeomagnetic study. New archeointensity results from this region could further be used to  
78 test (and later to improve) the reliability of the available global archeomagnetic field models  
79 (e.g. Licht et al., 2013; Pavón-Carrasco et al., 2014b; Nilsson et al., 2014.). In this paper, we  
80 report on new archeointensity data obtained from the Novgorod area, dated between c. 1100  
81 AD and c. 1700 AD.

82

## 83 **2. Archeomagnetic sampling**

84 All archeological fragments analyzed in this study consist of baked clay bricks  
85 collected from churches located in Novgorod (North-Western Russia) and its surroundings  
86 (Fig. 1). The oldest reference to the city of Novgorod goes back to the middle of the 9th  
87 century AD, making it one the most ancient Russian cities. During the 10th century AD,  
88 Novgorod was already a prosperous city because of its position on the trading route from the  
89 Varangians (i.e. the other name of Vikings) to the Greeks. Between the 11th and the 15th  
90 centuries, Novgorod was the capital city of the Novgorodian Republic, which extended from  
91 the Baltic to Northern Urals. This republic ended in 1478 AD when its territory became  
92 annexed to the state of Muscovy under the reign of Ivan III. During the republic period, many  
93 churches were built in the city of Novgorod and in nearby monasteries using bricks, local  
94 stones, or a combination of both. The construction date of these churches is known within a 1-  
95 7-yr uncertainty thanks to historical sources such as the Novgorod first chronicle (Fig. 2,  
96 Table 1; Nasonov, 1950; English translation in Michell and Forbes, 1914).

97 It is important to emphasize that the bricks used for construction are of local origin.  
98 The craftsmen benefited from abundant clay sources near Novgorod, which allowed the  
99 development of important pottery production activity, likely accompanied by brick  
100 manufacturing (e.g. Antipov and Gervais, 2015). The local origin of the bricks is also verified

101 through the discovery of a kiln at Ryurik Gorodishche, an area approximately 2 km south of  
102 the Novgorod center (Gervais and Lipatov 2003; Lipatov, 2005), whose brick production  
103 activity served to build the church of the Annunciation in the Gorodishche (site BGA01; Fig.  
104 2a, Table 1) in 1103 AD. Recently, the continuous activity of brick production in Novgorod  
105 with a regional distribution was further substantiated by the discovery of a ship carrying a  
106 load of bricks that sunk to the bottom of the Volkhov river (Antipov and Gervais, 2015).  
107 Interestingly, no evidence for an active brick market in Novgorod during the Middle Ages  
108 was found in the archives, nor for a large storage space for the fabricated bricks within the  
109 city. This indicates that the time delay between the production and the use of the bricks was  
110 most probably very short and the bricks were likely fired on request for specific buildings.

111 The archeomagnetic sampling of bricks was performed either on still standing  
112 churches or on vestiges found during excavations (Fig. 3). We note that the typology  
113 evolution of the bricks (see description and discussion in Antipov and Gervais, 2015)  
114 provided us with an additional guide for only selecting the bricks used in the original phase of  
115 the buildings, thus avoiding the bricks used in possible late renovations, or for identifying the  
116 bricks from different construction phases. Here we present new archeointensity data obtained  
117 from nine groups of brick fragments sampled from the remains of different churches. The  
118 bricks were dated from the beginning of the 12th century to the end of the 17th century AD  
119 (Table 1). The age distribution is inhomogeneous: four groups for the 12th and three for the  
120 14th centuries. The absence of fragments from the 13th century is linked to the Mongol  
121 invasion of 1238-1240 AD. Although the invasion did not destroy the city of Novgorod, it  
122 caused a marked slowdown in regional economic activity and thus led to a limited number of  
123 new constructions during most of this century.

124

125

### 126 **3. Acquisition of new archeointensity data**

#### 127 *3.1. Methods*

128 Archeointensity data were obtained using the experimental protocol developed for the  
129 Triaxe magnetometer (Le Goff and Gallet, 2004). The Triaxe is a vibrating sample  
130 magnetometer that allows continuous high-temperature (up to 670°C) magnetization  
131 measurements of a small (<1 cm<sup>3</sup>) cylindrical sample. It further allows the acquisition of a  
132 thermoremanent magnetization (TRM) in any direction and in a field intensity up to 200 μT.  
133 Le Goff and Gallet (2004) designed an automated routine for intensity determinations that  
134 involves a succession of five series of measurements performed between two temperatures  
135 referred to as T1 and T2. T1 is generally set to 150°C and T2, in the present study, was  
136 chosen between 440°C and 520°C depending on the specimens (see below). The NRM of the  
137 specimen is first demagnetized up to T2 (first series of measurements), while the thermal  
138 variations between T1 and T2 of the magnetization fraction still blocked above T2 are  
139 recorded twice during the second (between T2 and T1) and third series of measurements  
140 (between T1 and T2). A laboratory TRM is then acquired between T2 and T1 (fourth series of  
141 measurements), which is demagnetized up to T2 during the fifth series of measurements. The  
142 protocol ends with the cooling of the specimen down to room temperature. Intensity  
143 determinations are derived from the magnetization data acquired every 5°C during the first,  
144 third and fifth series of measurements, i.e. in the very same heating conditions between T1  
145 and T2. These measurements can be expressed through two ratios, which are multiplied by  
146 the field intensity used for laboratory-TRM acquisition, and defined as  $R(T_i)$  and  $R'(T_i)$  in Le  
147 Goff and Gallet (2004).  $R(T_i)$  is the ratio between the NRM and TRM fractions with  
148 unblocking temperatures between the running temperature  $T_i$  and T2, whereas  $R'(T_i)$  is the  
149 ratio between the NRM and TRM fractions unblocked between T1 and  $T_i$ . Le Goff and Gallet  
150 (2004) experimentally showed that  $R(T_i)$  is more prone to cooling rate effect over TRM

151 acquisition at higher temperatures than  $R'(Ti)$ . For this reason, the mean intensity values are  
152 derived at the specimen level from  $R'(Ti)$  data.

153 A great asset of the Triaxe protocol is that it avoids a correction for the TRM  
154 anisotropy effect because the laboratory TRM is acquired so that its direction is parallel to  
155 that of the NRM. A description of the procedure is provided in Le Goff and Gallet (2004) (see  
156 also in Genevey et al., 2008 for a general discussion on the TRM anisotropy effect). Thanks  
157 to numerous comparative tests with data obtained using more classical intensity techniques  
158 (Thellier-Aitken/-Coe/-IZZI methods; Thellier and Thellier, 1959; Aitken et al., 1988; Coe,  
159 1967; Yu et al., 2004) implying magnetization measurements at ambient temperature, it was  
160 also experimentally observed that the  $R'(Ti)$  intensity determinations account for the cooling  
161 rate effect on TRM acquisition (Le Goff and Gallet, 2004; Gallet and Le Goff, 2006; Genevey  
162 et al., 2009; Hartmann et al., 2010; 2011 and see in Section 3c below). Furthermore, any bias  
163 in the intensity data possibly induced by the presence of multi-domain grains in the specimen  
164 is mitigated because the laboratory TRM is acquired under similar conditions as those of the  
165 NRM.

166 In the present study, the reliability of the Triaxe data relies on the same set of selection  
167 criteria used by Genevey et al. (2013; 2016) and Hartmann et al. (2010; 2011). These criteria  
168 aim to insure the nominal paleomagnetic behavior described in Le Goff and Gallet (2004),  
169 which is characterized, in particular, by a “primary” univectorial magnetization component  
170 isolated between  $T1$  and  $T2$ , with the possibility to adjust a posteriori  $T1$  to a higher  
171 temperature (referred to  $T1'$ ) in case of a secondary magnetization component, and by rather  
172 constant  $R'(Ti)$  data over this temperature range (i.e. with an overall slope “ $S$ ” of less than  
173 10%). Rock magnetic analyses, including low-field magnetic susceptibility vs temperature,  
174 isothermal remanent magnetization (IRM) acquisition, hysteresis measurements, and three-

175 axis IRM demagnetization were also carried out on the fragments. These additional analyses  
176 constrain the nature and stability upon heating of their magnetic mineralogy.

177

### 178 *3.2. Magnetic mineralogy*

179 As a preliminary test for selecting the most promising fragments for intensity  
180 experiments, low-field magnetic susceptibility vs temperature curves were systematically  
181 acquired up to ~530-550°C on the whole collection using a Kappabridge MFK1 coupled with  
182 a CS4 thermal unit (Agico, Czech Republic). The first objective of these measurements was  
183 to test the thermal stability of the magnetic mineralogy inferred from the reversibility between  
184 the heating and cooling curves over the typical temperature range of intensity determinations.  
185 This is the reason why the thermomagnetic analyses were essentially performed up to a  
186 temperature relatively close to T<sub>2</sub>. Every fragment that was retained displays reversible  
187 behavior in susceptibility, as in Fig. 4a-e, whereas Fig. 4f illustrates a rejected fragment. We  
188 note that only two fragments were rejected at this step, which indicates magnetic stability  
189 upon heating of our collection of bricks. For a few fragments successfully analyzed in  
190 intensity, additional thermomagnetic measurements were also conducted at higher  
191 temperatures on new fresh powders, up to 700°C (insets in Fig. 4). They show a clear  
192 inflexion point between ~520°C and the Curie temperature of magnetite. The presence of  
193 hematite is also implied in several fragments (e.g. Fig. 4b).

194 In order to decipher the nature of the magnetic carriers in the fragments that met our  
195 archeointensity selection criteria, IRM and hysteresis measurements were performed on all  
196 the retained fragments. They were carried out up to 0.9 T using a Variable Field Translation  
197 Balance (VFTB; Peterson Instruments, Germany). IRM curves show that the magnetization is  
198 never saturated at 0.9 T, which indicates the presence of minerals with high-coercivity, such  
199 as hematite (Fig. 5a). We observe, however, a high variability in the IRM behavior. This



200 indicates variable proportions of this high-coercivity fraction against one characterized by  
201 lower coercivity. Some fragments (for instance PP01-05; PP01-12; BGA01-02; Fig. 5a)  
202 clearly exhibit around 0.1-0.2 T a plateau or a sharp inflection in the saturation curves. This  
203 likely emphasizes the joint presence of minerals from the (titano)magnetite family. In all  
204 cases, the hysteresis loops are constricted (Fig. 5b-d): this confirms that the magnetic  
205 mineralogy of our fragments consists of minerals with different coercivities.

206 For fragments fulfilling our archeointensity selection criteria (except six of them for  
207 which not enough material was remaining), we completed the previous measurements with  
208 thermal demagnetization of a three-axis IRM (1.2T, 0.4T, 0.2T) imparted in perpendicular  
209 directions (Lowrie, 1990). Three main categories of behavior are distinguished. In the first  
210 category (Fig. 5e), the low-coercivity fraction, most likely consisting of (titano)magnetite,  
211 largely dominates any other component of the magnetic mineralogy. The thermal  
212 demagnetization of this fraction is achieved around 550°C. This category represents about  
213 20% of the collection of fragments. In the second category (Fig. 5f), which is most frequent in  
214 our collection (about 50%), there is a higher proportion of high-coercivity minerals that is  
215 demagnetized around 200°C. This fraction is sometimes as large as that of low coercivity. In  
216 this case, the low-coercivity fraction predominates the magnetic signal between ~200°C and  
217 500/550°C. Although the presence of goethite cannot be excluded in our fragments on the  
218 basis of these experiments, it seems more probable that we observe the mineral of high  
219 coercivity and low unblocking temperature (HCLT), which is commonly present in  
220 archeological baked clays (e.g. McIntosh et al., 2011; Hartmann et al., 2011; Genevey et al.,  
221 2016). Lastly, the third category (about 30% of the collection) is characterized by a high-  
222 coercivity fraction, which remains present, and in a few cases, predominates the  
223 magnetization throughout the thermal demagnetization sometimes achieved above 600°C  
224 (Fig. 5g). Over a wide temperature range, the magnetization is thus carried both by low-

225 coercivity and high-coercivity minerals, which are most likely composed of (titano)magnetite  
226 and hematite.

227         As a synthesis, the rock magnetic analyses indicate that the magnetic mineralogy of  
228 our fragments includes three types of minerals with different coercivities and different  
229 unblocking temperatures in various proportions. These are likely (titano)magnetite, hematite,  
230 and the HCLT mineral. The latter can be a substituted form of hematite. It is worth  
231 mentioning that a similar combination of magnetic carriers is commonly found in  
232 archeomagnetic studies (e.g. Genevey et al., 2016).

233         Finally, we performed a series of specific archeointensity experiments on fragments  
234 belonging to the third IRM category described above. The aim was to ensure that, despite a  
235 significant proportion of hematite, these fragments provide a reliable value of the ancient  
236 geomagnetic field intensity. For these fragments, which are characterized by a magnetic  
237 mineralogy stable upon heating, a total pseudo-NRM was first acquired in a known laboratory  
238 field condition. In a second step, classical Triaxe archeointensity measurements were  
239 performed to analyze this pseudo-NRM. The latter allow to recover very precisely, to within a  
240 few %, the value of the field intensity used for the pseudo-NRM acquisition (Fig. S1 in  
241 supplementary material). These measurements therefore demonstrate that the hematite-related  
242 magnetization component does not significantly disturb the determination of the ancient field  
243 intensity that it is likely conveyed by the magnetization carried by (titano)magnetite.

244

### 245 *3.3. Cooling rate effect on TRM acquisition*

246         In several specimens, a rather specific behavior of the  $R(Ti)$  and  $R'(Ti)$  data was  
247 observed, that is characterized first, by a significant increase of the  $R(Ti)$  data with the  
248 temperatures and second, by a pronounced concave evolution of the  $R'(Ti)$  data (see two

249 examples in Fig. 6a,c). In several cases, the strong concavity of the  $R'(Ti)$  curves implied the  
250 rejection of the corresponding specimens.

251 Per the experiments performed by Le Goff et Gallet (2004), the significant increase in  
252  $R(Ti)$  data led us to suspect a strong cooling rate effect on TRM acquisition (see Section 5  
253 and Fig. 4 in Le Goff and Gallet, 2004, and in Genevey et al., 2008 for a more general  
254 discussion on the cooling effect on TRM acquisition). It is worth recalling that Le Goff and  
255 Gallet (2004) experimentally observed that the increasing trend in  $R(Ti)$  data can be linked to  
256 the fact that the cooling rate effect becomes stronger as the magnetization fractions with  
257 unblocking temperatures between  $T_i$  and  $T_2$  gradually decrease. Le Goff and Gallet (2004)  
258 further showed that this difficulty can be circumvented by considering  $R'(Ti)$  data relying on the  
259 magnetization fractions unblocked between  $T_1$  and  $T_i$ . In the present study, however, it was  
260 important to confirm this characteristic because the cooling rate effect appeared potentially  
261 strong. For this reason, we analyzed many fragments using (for different specimens) two  
262 cooling rates for the laboratory-TRM acquisition: 1- the one used for routine measurements  
263 carried out using the Triaxe, i.e. with a cooling rate fixed to 25°C/minute and 2- a cooling rate  
264 reduced to 2°C/minute (see details in Table S1 in supplementary material). In the latter case,  
265 the  $R'(Ti)$  data often exhibit a more suitable behavior with more constant values, while the  
266  $R(Ti)$  data show less increase over the temperature interval of analysis (Fig. 6b,d).

267 We then directly compared the intensity values computed at the group level (Fig. 7)  
268 using either the 25°C/minute cooling rate or the 2°C/minute cooling rate. This comparison  
269 shows no statistical significance in the difference, which remains within 5% when the  
270 intensity determinations obey our selection criteria. Moreover, on average (31 fragments) the  
271 differences in intensity at the fragment level relative to the values obtained using a cooling  
272 rate of 25°C/minute are also insignificant:  $1.5 \pm 2.8\%$ . Nevertheless, the use of a slow cooling  
273 rate of 2°C/minute allowed us to retain several fragments that would have been rejected

274 otherwise. This led us to retain the group of fragments GYU01, for which one fragment  
275 among the three was only successfully analyzed using the slow cooling rate (GYU01-04;  
276 Table S1 in supplementary material). Hereafter, we will therefore determine mean intensity  
277 values at the fragment level by combining the values obtained whatever the cooling rate  
278 applied. Finally we note that for some specimens, T2 was chosen relatively low (440°C;  
279 Table S1 in supplementary material), assuming that the cooling rate dependence on TRM  
280 acquisition was more pronounced for the magnetization fraction unblocked at high  
281 temperatures (Le Goff and Gallet, 2004).

282

### 283 *3.4. Archeointensity data*

284 Our experiments allowed us to obtain archeointensity data satisfying our selection  
285 criteria from 165 specimens (of a total of 337 specimens whose magnetization was strong  
286 enough for the Triaxe magnetometer). These specimens are from 40 different fragments, with  
287 usually 3 to 4 specimens successfully analyzed per fragment (see Table 1 in Supplementary  
288 material). This corresponds to a rate of success comprised between 42% and 67% depending  
289 on the groups of fragments (Table S1 in supplementary material). Failures were linked, in  
290 equal proportion, to a strong concavity of the  $R'(Ti)$  curve (Fig. 6c), a large slope of the  
291  $R'(Ti)$  curve or to a difference between specimen values from a same fragment larger than our  
292 5% limit. Typical examples of thermal demagnetization data for successful specimens are  
293 reported in Fig. S2 (in supplementary material). Mean intensity values were derived for nine  
294 groups of fragments, with a minimum number of three fragments per group (VS01, GYU01).  
295 This number increases up to five for four groups (DM03, DM02, BGA01, SH01) and six for  
296 group PP01. Fig. 8 illustrates the archeointensity data obtained from six different groups of  
297 fragments (one panel per group). In this representation, each curve exhibits the  $R'(Ti)$  data  
298 obtained for one specimen. The curves also represent the scatter in the data obtained from

299 each group. Here, we observe that the variability is quite weak, which was expected given the  
300 excellent temporal homogeneity of the fragments from each group.

301 As in all the previous studies dealing with Triaxe intensity data (e.g. Genevey et al,  
302 2013; Gallet et al, 2014), we estimated a mean archeointensity value for each group of  
303 fragments via first the averaging of the  $R'(Ti)$  data obtained for each specimen, then the  
304 averaging of these specimen values at the level of each fragment, and finally the averaging of  
305 the fragment values at the group level. The group-mean archeointensity results are well  
306 defined, with standard deviations consistently less than  $2.6 \mu\text{T}$  and not exceeding 5% of the  
307 corresponding group-mean value (between 1.2% and 4.2%). They range from  $66.1 \pm 1.9 \mu\text{T}$  to  
308  $48.7 \pm 1.6 \mu\text{T}$ , with an overall decrease of the geomagnetic field intensities between the 12th  
309 and 17th centuries AD (Table 1; Fig. 9).

310

#### 311 **4. Discussion**

312 Fig. 9a shows the data available within a radius of 700 km around Novgorod (grey  
313 dots). Apart from the new archeointensity results reported in the present study, the previous  
314 data were principally obtained from two areas (Fig. 1a) around Moscow and Vologda (~500  
315 km from Novgorod). Although the data were obtained over 30-years-ago (Burlatskaya et al.,  
316 1986), partial-TRM checks were used most often to test the stability of the magnetic  
317 mineralogy on heating (Genevey et al., 2008). Here we only retained the data with partial-  
318 TRM checks and those for which the standard deviation is less than 15% of the corresponding  
319 mean intensity value. Note that the corresponding fragments were collected from architectural  
320 bricks, a material for which the TRM anisotropy effect is expected to be weak (e.g. Genevey  
321 et al., 2008). A color code in Fig. 9a allows one to distinguish between results obtained from  
322 two or more independent archeological artifacts. Two main remarks can be made about these  
323 data. Firstly, within the ~1500-1800 AD time interval, they are very scattered regardless of

324 the number of fragments or specimens used to estimate the mean intensity values, which  
325 prevents a clear determination of the geomagnetic field intensity evolution. Such a scatter  
326 clearly casts doubt on the reliability of at least some of these data. Secondly, no result was  
327 available up to now from North-Western Russia for the ~1000-1400 AD time interval.

328         While our new data exhibits an overall decreasing trend in geomagnetic field intensity  
329 over the time interval of concern, they do not show a variability that could indicate the  
330 occurrence of rapid and large-amplitude intensity fluctuations in North-Western Russia  
331 during the past millennium. In this respect, although it is acknowledged that the present  
332 dataset contains only nine archeointensity values, they do not corroborate the large variations  
333 observed in the Balkan region (700 km around Thessaloniki; Tema and Kondopoulou, 2011;  
334 Kovacheva et al., 2014). This difference is illustrated in Fig. 9a, where the Balkan data (light  
335 violet squares) are reported after their transfer to the latitude of Novgorod using the Virtual  
336 Axial Dipole Moment approximation. Here we recognize that this approach adds uncertainties  
337 on the transferred values (e.g. Casas and Inconato, 2007); however we assume that they  
338 remain relatively limited compared to the experimental and age uncertainties of the data. For  
339 the latter dataset, a color code is used to distinguish between results with and without partial-  
340 TRM checks (see discussion in Genevey et al., 2013; 2016). This distinction does not,  
341 however, allow one to detect any difference in the nature of the intensity fluctuations in the  
342 Balkans. In contrast, the Novgorod results appear in better agreement with the average  
343 geomagnetic field intensity variation curve for Western Europe (700 km around Paris; blue  
344 curve in Fig. 9a), also transferred to the latitude of Novgorod, determined by Genevey et al.  
345 (2013; 2016). However, the available data are still not numerous enough to show the  
346 occurrence of similar short-lasting relative maxima in North-Western Russia as those  
347 observed in Western Europe, i.e. dated from the 12th century, the second half of the 14th  
348 century and around 1600 AD (Genevey et al., 2016). At present, the archeointensity dataset

349 from the Novgorod area is more compatible with homogeneous geomagnetic field intensity  
350 variations throughout Europe over the past millennium (e.g. Pavón-Carrasco et al., 2014a).

351 In Fig. 9b, the new archeointensity data are also compared with the expected intensity  
352 values computed at Novgorod from recent global archeomagnetic field models (i.e. A\_FM,  
353 Licht et al., 2013; SCHA\_DIF.14k, Pavón-Carrasco et al., 2014b; pfm9k.1a, Nilsson et al.,  
354 2014). Note that the curve derived from pfm9k.1a (brown curve) displays smoother variations  
355 than those from the two other models (green curve, A\_FM; orange curve, SCHA-DIF.14k),  
356 which is due to the use of sedimentary, volcanic and archeological data by Nilsson et al.  
357 (2014) (for instance, see discussion in Licht et al., 2013). Nevertheless, in all three cases, the  
358 models quasi-systematically predict intensity values that are statistically higher than the data  
359 obtained in the Novgorod area. This indicates that the global field models need to be revised  
360 to correct for this intensity over-estimation in North-Western Russia. It is possible that at least  
361 a part of this offset originates from the cooling rate effect, which was considered only for a  
362 small proportion of the archeointensity data used for field modeling (Genevey et al., 2008;  
363 Brown et al., 2015).

364 The most recent archeointensity result obtained in Novgorod, i.e. from group DM03  
365 precisely dated to the end of the 17th century (Table 1), is also of special interest for field  
366 modeling. Its value is lower by  $\sim 5 \mu\text{T}$  than the expected intensity around the same epoch  
367 which was derived from the historical geomagnetic field modeling referred to as gufm1 (black  
368 curve in Fig. 9b; Jackson et al., 2000). Briefly, it is worth recalling that the latter field models  
369 were built using magnetic field measurements made by mariners and performed in a few land  
370 observatories (e.g., Jonkers et al., 2003), and assuming a linearly decreasing geocentric axial  
371 dipole field moment (term  $g_1^0$ ) from  $\sim 1600$  AD to the present (Barraclough, 1974). Such  
372 hypothesis made for the 1600-1840-time interval (i.e. beyond the first direct intensity  
373 measurements) is not confirmed here. Even though differences appear less pronounced, our

374 value also fails to confirm a constant -or nearly constant  $g_1^0$  evolution between ~1600 and  
375 1840, as previously proposed by Finlay (2008) and Gubbins et al. (2006), respectively (Fig.  
376 9b). On the other hand, its age cannot help deciphering the oscillatory  $g_1^0$  evolution suggested  
377 by Genevey et al. (2009) over the past four centuries (see also Hartmann et al., 2011 for  
378 Brazilian data). More archeomagnetic data are clearly needed to strengthen this important  
379 issue.

380

## 381 **5. Conclusions**

382 This study is part of a project, which aims to acquire archeomagnetic data acquisition  
383 from Central and North-Western Russia. Previous studies were consistently made during the  
384 70s and 80s, but unfortunately stopped for many years. At the same time, other Western  
385 Eurasian regions benefited from a strong development in archeomagnetism research activity.

386 We investigated several groups of architectural brick fragments collected from old  
387 churches in the Novgorod area. These groups are precisely dated between the 12th and 17th  
388 century AD.

389 Archeointensity analyses were carried out using the experimental protocol developed  
390 for the Triaxe magnetometer. They allow us to obtain nine new mean archeointensity data,  
391 derived from 40 different fragments and 165 analyzed specimens.

392 These data show an overall decreasing trend in geomagnetic field intensity over the  
393 past millennium, with no evidence of rapid variations with large amplitude such as those  
394 proposed from the Balkans (e.g. Tema and Kondopoulou, 2011; Kovacheva et al., 2014).  
395 They are more compatible with the French geomagnetic field intensity variation curve  
396 proposed by Genevey et al. (2016), after its transfer to the latitude of Novgorod. Should this  
397 result persist in future archeointensity data collections and analyses, the intensity secular



398 variation would have remained homogeneous across all Europe during at least the past  
399 millennium.

400 An intriguing observation is that our Novgorod results are lower than the intensity  
401 values predicted from archeomagnetic field models. We suggest that the observed differences,  
402 at least in part, originate from the cooling rate effect on TRM acquisition, the latter not  
403 considered in most of the data used for the construction of the models.

404 Finally, we note that a result dated to the end of the 17<sup>th</sup> century is not compatible with  
405 the expected intensity value derived from the gufm1 model (Jackson et al., 2000), which  
406 assumes a linear decrease of the axial dipole moment over the past four centuries.

407

#### 408 **Acknowledgments**

409 This study was financed by grant N 14.Z50.31.0017 of the Russian Ministry of Science and  
410 Education. We are very grateful to Maxime Le Goff for his unwavering technical assistance.  
411 We thank two anonymous reviewers for their helpful comments. This is IPGP contribution  
412 no. 3842.

413

#### 414 **References**

415 Aitken, M. J., Allsop, A. L., Bussell, G. D., Winter, M. B., 1988. Determination of the  
416 intensity of the Earth's magnetic field during archaeological times: Reliability of the  
417 Thellier technique. *Rev. Geophys.* 26, 3-12.

418 Aitken, M. J., Allsop, A. L., Bussell, G. D., Liritzis, Y., Winter, M. B., 1989. Geomagnetic  
419 intensity measurements using bricks from Greek churches of the first and second  
420 millennia A.D.. *Archaeometry* 31, 77-87.

421 Antipov, I., Gervais, A., 2015. The bricks from St Nicholas church at Lipno near Novgorod  
422 (1292) and the origins of the new Novgorodian building tradition. *Estonian Journal of*  
423 *Archaeology* 19, 58-7.

424 Barraclough, D., 1974. Spherical harmonic analysis of the geomagnetic field for eight epochs  
425 between 1600 and 1910. *Geophys. J. R. Astron. Soc.* 43, 497–513.

426 Brown, M. C., Donadini, F., Korte, M., Nilsson, Korhonen, K., Lodge, A., Lengyel, S. N.,  
427 Constable, C. G., 2015. GEOMAGIA50.v3: 1. General structure and modifications to  
428 the archeological and volcanic database. *Earth Planet and Space* 67, 1-31.

429 Burlatskaya, S. P., Nachasova, I.E., Didenko, E. J., Shelestun, N. K., 1986. Archeomagnetic  
430 determinations of geomagnetic field elements. *Sov. Geophys. Comm. of the USRR*  
431 *Acad. of Sci., Moscow*.

432 Casas, L., Incoronato, A., 2007. Distribution analysis of errors due to relocation of  
433 geomagnetic data using the ‘Conversion via Pole’ (CVP) method: implications on  
434 archeomagnetic data. *Geophys. J. Int.* 169, 448–454.

435 Coe, R. S., 1967. Paleo-Intensities of the Earth's magnetic field determined from Tertiary and  
436 Quaternary Rocks. *J. Geophys. Res.* 72, 3247–3262.

437 De Marco, E., Spatharas, V., Gómez-Paccard, M., Chauvin, A., Kondopoulou, D., 2008. New  
438 archaeointensity results from archaeological sites and variation of the geomagnetic field  
439 intensity for the last 7 millennia in Greece. *Phys. Chem. Earth* 33, 578–595.

440 Finlay, C.C., 2008. Historical variation of the geomagnetic axial dipole. *Phys. Earth Planet.*  
441 *Inter.* 170, 1-14.

442 Gallet, Y., Genevey, A., Le Goff, L., 2002. Three millennia of directional variation of the  
443 Earth’s magnetic field in western Europe as revealed by archeological artefacts. *Phys.*  
444 *Earth Planet. Inter.* 131, 81-89.

445 Gallet, Y., Le Goff, M., 2006. High-temperature archeointensity measurements from  
446 Mesopotamia. *Earth Planet. Sci. Lett.* 241, 159-173.

447 Gallet, Y., Genevey, A., Le Goff, M., Warmé, N., Gran-Aymerich, J., Lefèvre, A., 2009. On  
448 the use of archeology in geomagnetism, and vice-versa: Recent developments in  
449 archeomagnetism. *C. R. Physique*, 10 630–648.

450 Gallet, Y., D’Andrea, M., Genevey, A., Pinnock, F., Le Goff, M., Matthiae, P., 2014.  
451 Archaeomagnetism at Ebla (Tell Mardikh, Syria). New data on geomagnetic field  
452 intensity variations in the Near East during the Bronze Age. *J. Archaeol. Sci.* 42, 295-  
453 304.

454 Genevey, A., Gallet, Y., Constable, C., Korte, M., Hulot, G., 2008. ArcheoInt: An upgraded  
455 compilation of geomagnetic field intensity data for the past ten millennia and its  
456 application to the recovery of the past dipole moment. *Geochem. Geophys. Geosys.*  
457 9(4), Q04038.

458 Genevey, A., Gallet, Y., Rosen, J., Le Goff, M., 2009. Evidence for rapid geomagnetic field  
459 intensity variations in Western Europe over the past 800 years from new archeointensity  
460 French data. *Earth Planet. Sci. Lett.* 284, 132-143.

461 Genevey, A., Gallet, Y., Thébault, E., Jesset, S., Le Goff, M., 2013. Geomagnetic field  
462 intensity variations in Western Europe over the past 1100 years. *Geochem. Geophys.*  
463 *Geosyst.* 14/8, 2858-2872.

464 Genevey, A., Gallet, Y., Jesset, S., Thébault, E., Bouillon, J., Lefèvre, A., Le Goff, M., 2016.  
465 New archeointensity data from French Early Medieval ceramic production (6th-10th  
466 century AD). Tracing 1500 years of geomagnetic field intensity variations in Western  
467 Europe. *Phys. Earth Planet. Inter.* 257, 205-219.

468 Gervais, A. V., Lipatov A. A., 2003. The interpretation problems of the kiln near the  
469 Annunciation church on Gorodishche (in Russian). In *Novgorod i Novgorodskaia*  
470 *zemlia. Istorica i archeologia*. V. Novgorod 17, 344–350.

471 Gómez-Paccard, M., Chauvin, A., Lanos, P., Thiriot, J., 2008. New archeointensity data from  
472 Spain and the geomagnetic dipole moment in western Europe over the past 2000 years.  
473 *J. Geophys. Res.*, 113, B09103.

474 Gómez-Paccard, M., Chauvin, A., Lanos, P., Dufresne, P., Kovacheva, M., Hill, M. J.,  
475 Beamud, E., Blain, S., Bouvier, A., Guibert, P., and Archaeological Working Team,  
476 2012. Improving our knowledge of rapid geomagnetic field intensity changes observed  
477 in Europe between 200 and 1400 AD. *Earth Planet. Sci. Lett.* 355–356, 131–143.

478 Gómez-Paccard, M., Osete, M.L., Chauvin, A., Pavón-Carrasco F.J., Pérez-Asensio, M.,  
479 Jiménez, P., Lanos, P., 2016. New constraints on the most significant paleointensity  
480 change in Western Europe over the last two millennia. A non-dipolar origin?. *Earth*  
481 *Planet. Sci. Lett.* 454, 55-64.

482 Gubbins, D., Jones, A.L., Finlay, C.C., 2006. Fall in Earth's magnetic field is erratic. *Science*  
483 312, 900-902.

484 Hartmann, G., Genevey, A., Gallet, Y., Trindade, R., Etchevarne, C., Le Goff, M., Afonso,  
485 M., 2010. Archeointensity in Northeast Brazil over the past five centuries. *Earth Planet.*  
486 *Sci. Lett.* 296, 340-352.

487 Hartmann, G., Genevey, A., Gallet, Y., Trindade, R., Le Goff, M., Najjar, R., Etchevarne, C.,  
488 Afonso, M., 2011. New historical archeointensity data from Brazil : Evidence for a  
489 large regional non-dipole field contribution over the past few centuries. *Earth Planet.*  
490 *Sci. Lett.* 306, 66-76.

491 Hervé, G., Chauvin, A. Lanos P., 2013a. Geomagnetic field variations in Western Europe  
492 from 1500 BC to 200 AD. Part I: Directional secular variation curve. *Phys. Earth*  
493 *Planet. Inter.* 218, 1-13.

494 Hervé, G., Chauvin, A. Lanos P., 2013b. Geomagnetic field variations in Western Europe  
495 from 1500 BC to 200 AD. Part II: New intensity secular variation curve. *Phys. Earth*  
496 *Planet. Inter.* 218, 51-65.

497 Hervé, G., Chauvin, A., Milcent, P.-Y., Tramon, A., 2016. Archaeointensity study of five  
498 Late Bronze Age fireplaces from Corent (Auvergne, France). *J. Archaeol. Sci.: Reports*  
499 7, 414-419.

500 Jackson, A., Jonkers, A., Walker, M., 2000. Four centuries of geomagnetic secular variation  
501 from historical records. *Philos. Trans. R. Soc. Lond. Ser. A* 358, 957-990.

502 Jonkers, A. R. T., Jackson, A., Murray, A., 2003. Four centuries of geomagnetic data from  
503 historical records. *Rev. Geophys.* 41, 1006.

504 Kovacheva, M., Boyadziev, Y., Kostadinova-Avramova, M., Jordanova, N., Donadini, F.,  
505 2009. Updated archeomagnetic data set of the past eight millennia from the Sofia  
506 laboratory, Bulgaria. *Geochem. Geophys. Geosyst.* 10, Q05002,  
507 doi:10.1029/2008GC002347.

508 Kovacheva, M., Kostadinova-Avramova, M., Jordanova, N., Lanos, P., Boyadziev, Y., 2014.  
509 Extended and revised archaeomagnetic database and secular variation curves from  
510 Bulgaria for the last eight millennia. *Phys. Earth Planet. Inter.* 236, 79-94, doi:  
511 10.1016/j.pepi.2014.07.002.

512 Le Goff, M., Gallet, Y., 2004. A new three-axis vibrating sample magnetometer for  
513 continuous high-temperature magnetization measurements: applications to paleo- and  
514 archeo-intensity determinations. *Earth Planet. Sci. Lett.* 229, 31-43.

- 515 Licht, A., Hulot, G., Gallet, Y., Thébault, E., 2013. Ensembles of low degree archeomagnetic  
516 field models for the past three millennia. *Phys. Earth Planet. Inter.* 224, 38-67.
- 517 Lipatov, A. A., 2005. The kiln from Gorodishche (1988 excavations) in the context of lime  
518 manufacturing in Byzantine, Western Europe and Ancient Russia (in Russian). In  
519 Nosov E. N., Gorunova V.M., Plokhov A.V. Eds., *Gorodishche pod Novgorodom i*  
520 *poselenia Severnogo Priilmeniya (Noviye materialy i issledovaniia)*. Saint-Petersburg,  
521 Dmitrii Bulanin, 258-393.
- 522 Lowrie, W., 1990. Identification of ferromagnetic minerals in a rock by coercivity and  
523 unblocking temperatures properties. *Geophys. Res. Lett.*, 17, 159–162.
- 524 McIntosh, G., Kovacheva, M., Catanzariti, G., Donadini, F., Lopez, M. L. O., 2011. High  
525 coercivity remanence in baked clay materials used in archeomagnetism. *Geochem.*  
526 *Geophys. Geosyst.*, 12, Q02003.
- 527 Michell, R., Forbes, N., 1914. The chronicle of Novgorod 1016-1471 (translated from the  
528 Russian). *Camden Third Series Vol. XXV*, London Office of the Society, pp. 237.
- 529 Nachasova, I. YE., 1972. Magnetic field in the Moscow area from 1480 to 1840 (Engl.  
530 Transl). *Geomagn. Aeron.* 12, 277-280.
- 531 Nasonov A. N. (Ed.), 1950. *Novgorodskaya Pervaya letopis* (in Russian). Izdatelstvo  
532 Akademii nauk SSSR, Moscow–Leningrad, pp. 642.
- 533 Nilsson, A., Holme, R., Korte, M., Suttie, N., Hill, M., 2014. Reconstructing Holocene  
534 geomagnetic field variation: New methods, models and implications, *Geophys. J. Int.*  
535 198, 229-248.
- 536 Pavón-Carrasco, F. J., Gómez-Paccard, M., Hervé, G., Osete López, M.L., and A. Chauvin,  
537 A., 2014a. Intensity of the geomagnetic field in Europe for the last 3 ka: Influence of

538 data quality on geomagnetic field modeling. *Geochem. Geophys. Geosyst.* 15, 2515-  
539 2530.

540 Pavón-Carrasco, F. J., Osete López, M. L., Torta, J. M., De Santis, A., 2014b. A geomagnetic  
541 field model for the Holocene based on archaeomagnetic and lava flow data. *Earth*  
542 *Planet. Sci. Lett.* 388, 98–109.

543 Pesonen, L. J., Leino, M. A. H., Nevanlinna, H., 1995. Archaeomagnetic intensity in Finland  
544 during the last 6400 years: Evidence for a latitude-dependent nondipole field at  
545 approximately AD 500. *J. Geomagn. Geoelectr.* 47, 19–40.

546 Rybina, E. A., 1992. Trade links of medieval Novgorod established through archaeological  
547 data. In: *The archaeology of Novgorod, Russia. Recent results from the town and its*  
548 *hinterland.* Eastern Press, Ltd, Lincoln, 193–205.

549 Rybina, E. A., 2001. Frühe “joint-ventures”. *Die Beziehungen Novgorods im Ostseeraum.* In:  
550 M. Müller-Wille u.a. (Hrsg.), *Novgorod. Das mittelalterliche Zentrum und sein Umland*  
551 *im Norden Russlands. Studien zur Siedlungsgeschichte und Archäologie der*  
552 *Ostseegebiete.* 1. Neumünster, 291–308.

553 Spassov, S., Valet, J.-P. , Kondopoulou, D., Zananiri, I., Casas, L., Le Goff, M., 2010. Rock  
554 magnetic property and paleointensity determination on historical Santorini lava flows.  
555 *Geochem. Geophys. Geosyst.* 11, Q07006, doi:10.1029/2009GC003006.

556 Tema, E., Kondopoulou, D., 2011. Secular variation of the Earth’s magnetic field in the  
557 Balkan region during the last eight millennia based on archaeomagnetic data. *Geophys.*  
558 *J. Int.* 186(2), 603-614.

559 Tema, E., Gómez-Paccard , M., Kondopoulou, D., Ylenia, A., 2012. Intensity of the Earth’s  
560 magnetic field in Greece during the last five millennia: New data from Greek pottery.  
561 *Phys. Earth Planet. Inter.* 202–203, 14–26.

562 Tema, E., Morales, J., Goguitchaichvili, A., Camps, P., 2013. New archaeointensity data from  
563 Italy and geomagnetic field intensity variation in the Italian Peninsula. *Geophys. J. Int.*  
564 193, 603–614.

565 Thellier, E., Thellier, O., 1959. Sur l'intensité du champ magnétique terrestre dans le passé  
566 historique et géologique. *Ann. Géophys.* 15, 285-376.

567 Yu, Y., Tauxe, L., Genevey, A., 2004. Toward an optimal geomagnetic field intensity  
568 determination technique. *Geochem. Geophys. Geosyst.*, 5, Q02H07.

569

570

### Figure captions

571

572 **Fig. 1** (a) Location map of the city of Novgorod. (b) Map that identifies the location of groups  
573 of architectural brick fragments collected in the Novgorod area. 1- Church of the  
574 Annunciation in the Gorodishche (group BGA01), 2- Monastery church of St. Georgi (group  
575 GYU01), 3- Church to the Holy Apostels Peter and Paul in Silnishche (group PP01), 4-  
576 Transfiguration church on Nereditsa hill (group SN01), 5- Holy Virgin Protection church of  
577 Shilov Monastery (group SH01), 6,9- Church of the Holy Resurrection on the Derevyanitza  
578 river (groups DM02 and DM03), 7- Church of St. Andrew the Holy Fool on Sitka (group  
579 AS01), 8- Cathedral of Our Lady of Vladimir of Syrkov Monastery (group VS01).

580

581 **Fig. 2** Examples of dating via details found in the Novgorod First Chronicle (translation from  
582 Michell and Forbes, 1914) for two of our groups of brick fragments. (a) Dating of the church  
583 of the Annunciation in the Gorodishche (BGA01). (b) Dating of the church of the Holy  
584 Apostels Peter and Paul in Silnishche (PP01).

585



586 **Fig. 3** Archeological context of four groups of brick fragments. (a) SN01; (b) DM02; (c)  
587 AS01; (d) SH01. See details in Fig. 1 and Table 1.

588

589 **Fig. 4** Examples of low-field magnetic susceptibility versus temperature curves for our  
590 collection of fragments. The heating/cooling curves are in red/blue. The maximum  
591 temperatures were chosen relatively close to temperature T<sub>2</sub> used for archeointensity  
592 experiments (see text). The data shown in the insets were obtained on fresh powders from the  
593 same fragments up to 700°C.

594

595 **Fig. 5** IRM experiments conducted on the fragments fulfilling the criteria used to select the  
596 archeointensity results. (a) IRM curves obtained up to 0.9 T (see color code in the Figure). (b-  
597 d) Examples of hysteresis loops illustrating the three categories of IRM behavior discussed in  
598 the text. (e-g) Examples of thermal demagnetization of three-axis IRM acquired along three  
599 perpendicular directions (1.2 T, 0.4 T, 0.2 T; Lowrie, 1990).

600

601 **Fig. 6** Cooling rate effect on the shape of the R(Ti) and R'(Ti) curves for fragments PP01-04  
602 (a,b) and AS01-04 (c,d). The data were obtained using a cooling rate of 25°C/minute (a,c) vs  
603 a cooling rate of 2°C/minute (b,d). In red (resp. black) the R'(Ti) (resp. R(Ti)) data (Le Goff  
604 and Gallet, 2004). See text for further explanations.

605

606 **Fig. 7** Comparison between group-mean intensity values estimated using cooling rates of  
607 25°C/minute and 2°C/minute. The different symbols distinguish between mean intensity  
608 values determined at the fragment group level from a minimum of three different fragments  
609 (black dots) or from only two fragments (white dots; see supplementary Table S1).

610

611 **Fig. 8** Archeointensity results obtained for six different groups of brick fragments. In each  
612 panel, each curve represents the  $R'(Ti)$  data obtained for one specimen (see color code on the  
613 figure). These data are first averaged at the specimen level, then a mean intensity value is  
614 estimated at the fragment level and the latter are averaged at the group level.

615

616 **Fig. 9** Geomagnetic field intensity variations in the North-Western part of Russia over the  
617 past millennium. (a) Our new archeointensity data (red diamond) are compared with the data  
618 transferred to the latitude of Novgorod presently available within a radius of 700 km around  
619 Novgorod (grey dots, Nachasova, 1972; Burlatskaya et al., 1986; Pesonen et al., 1995;  
620 Kovacheva et al., 2009) and from the Balkans (light violet squares, Aitken et al., 1988, 1989;  
621 De Marco et al., 2008; Spassov et al., 2010; Kovacheva et al., 2014). The blue curve exhibits  
622 the average intensity variation curve obtained for Western Europe (Genevey et al., 2016) after  
623 its transfer to the latitude of Novgorod. (b) A comparison is also performed with the  
624 geomagnetic field intensity values expected in Novgorod from different global  
625 archeo/geomagnetic field models (see details and color code on the figure).

626

627

### Table caption

628

629 **Table 1** New archeointensity data obtained in Novgorod area. Location, name and dating of  
630 the different churches are indicated in columns 2 (Latitude), 3 (Longitude), 4 (Site) and 5  
631 (Age). N/fragment (6<sup>th</sup> column) and n/specimen (7<sup>th</sup> column): number of fragments and  
632 specimens used for group-mean intensity computations.  $F_{mean} \pm \sigma F$  ( $\mu T$ ) (8<sup>th</sup> column): mean  
633 intensity and its standard deviation obtained for each group of brick fragments.

634

635

## Supplementary Information

636  
637  
638  
639  
640  
641  
642  
643  
644  
645  
646  
647  
648  
649  
650  
651  
652  
653  
654  
655  
656  
657  
658  
659  
660

**Fig. S1** Archeointensity experiments performed on a pseudo-NRM acquired in known field conditions for two fragments (a) DM02-02 and (b) SH01-06 showing a large fraction of magnetization carried by hematite. The pseudo-NRM was acquired in a field of 60  $\mu\text{T}$  and using a cooling rate of 25°C/minute. Triaxe experiments were conducted using the same field and cooling conditions. In red (resp. black) the  $R'(Ti)$  (resp.  $R(Ti)$ ) data (Le Goff and Gallet, 2004). See text for further explanations

**Fig. S2** Typical examples of thermal demagnetization of the NRM carried by specimens successfully analyzed using the Triaxe protocol (first series of measurements acquired in that protocol; see in Section 3.a and in Le Goff and Gallet, 2004). In each case, the red dot indicates the closest temperature to  $T1'$  used for archeointensity determinations.

**Table S1** Archeointensity data obtained in Novgorod area both at the specimen and fragment levels. Column description: Fragment identification; Specimen identification;  $T1$ - $T2$ , temperature interval (in °C) for intensity determination;  $H_{lab}$ , laboratory field used for TRM acquisition in  $\mu\text{T}$ ; Cooling rate (°C/minute), cooling rate used for TRM acquisition; NRM  $T1$  ( $T1'$ ) (%), fraction of NRM from  $T1'$  involved in intensity determination (with  $T1 < T1' < T2$ ); Slope  $R'$  (%), slope of the  $R'(Ti)$  data within the temperature interval of analysis;  $F$ , intensity value in  $\mu\text{T}$  derived for each specimen;  $F_{mean}$  value per fragment  $\pm \sigma_H$ , mean intensity in  $\mu\text{T}$  computed at the fragment level with its standard deviation. \*( $N1/N2/N3$ ),  $N1$ : number of fragments investigated,  $N2$ : number of fragments whose magnetization was strong enough for allowing Triaxe measurements,  $N3$ : number of fragments obeying our selection criteria.

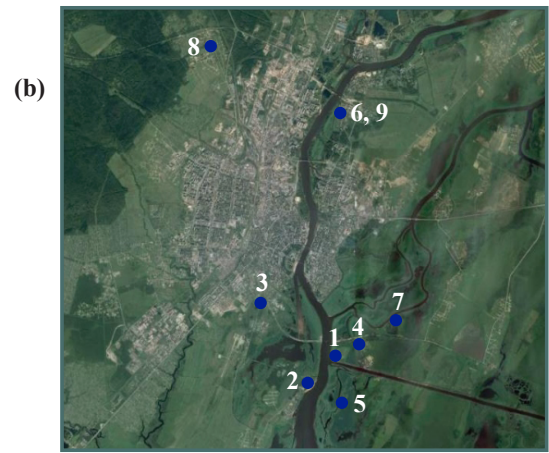


Figure 1

**(a)**

A.D. 1103. A.M.6611 All the brethren Knyazes of the Russian Land went against the Polovets people to the Suten, and delected them, and captured the belongings of their Knyaz. The same year the Mordva<sup>6</sup> people defeated Yaroslav at Murom. The same year Knyaz Mstislav founded the Church of the Annunciation in the Gorodishche<sup>6</sup>.

**(b)**

A.D. 1185. A.M. 6693. On the 1st day of May, at the 10th hour of the day, at evening bell, the sun grew dark, for an hour or more, and there were the stars; then it stone out again, and we were glad. On the 6th of the same month the people of Luki founded a stone church to the holy Apostels Peter and Paul in Silnishche. The same year Miloneg founded the stone church of the Holy Ascension under Vladyka Ilya and Knyaz Mstislav Davidovits. And in the winter David went Polotsk with the men of Novgorod and of Smolensk, and having made peace returned through Ymenets.

Figure 2



Figure 3

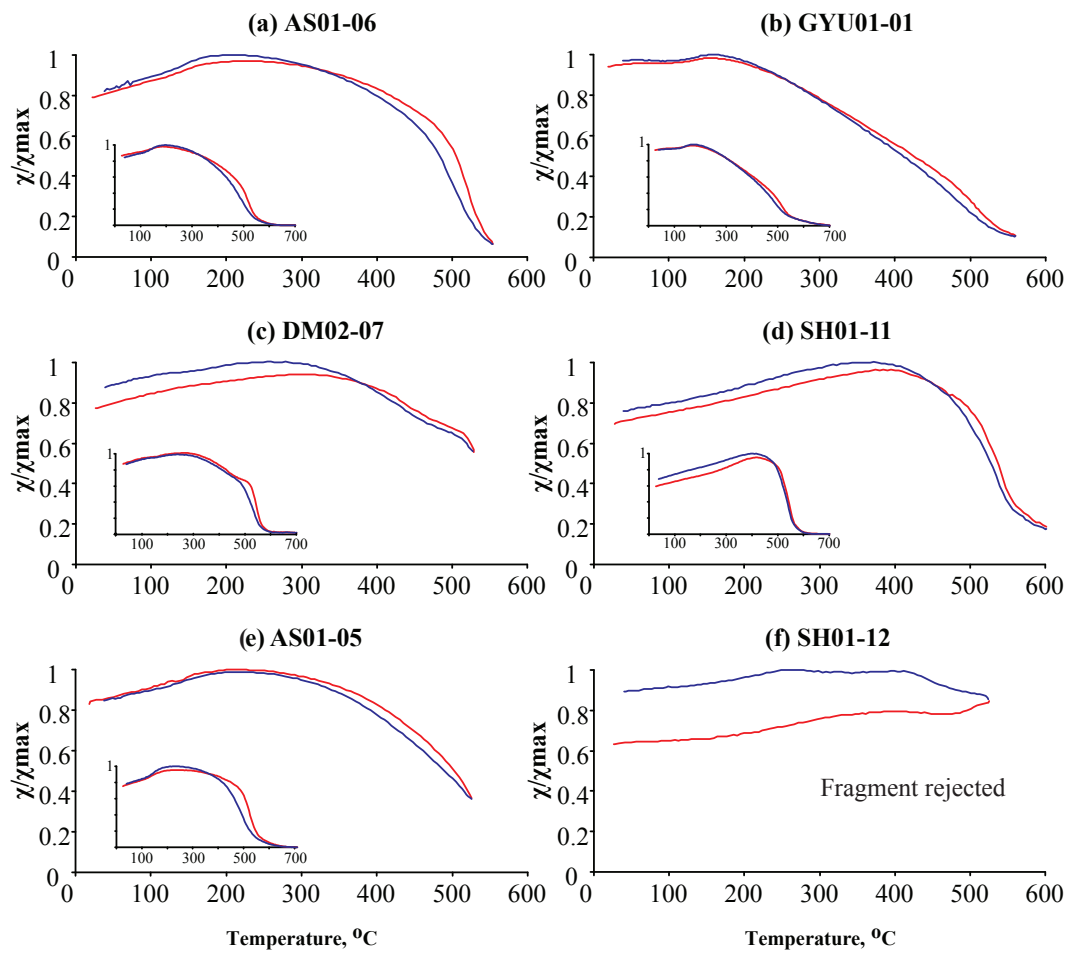


Figure 4

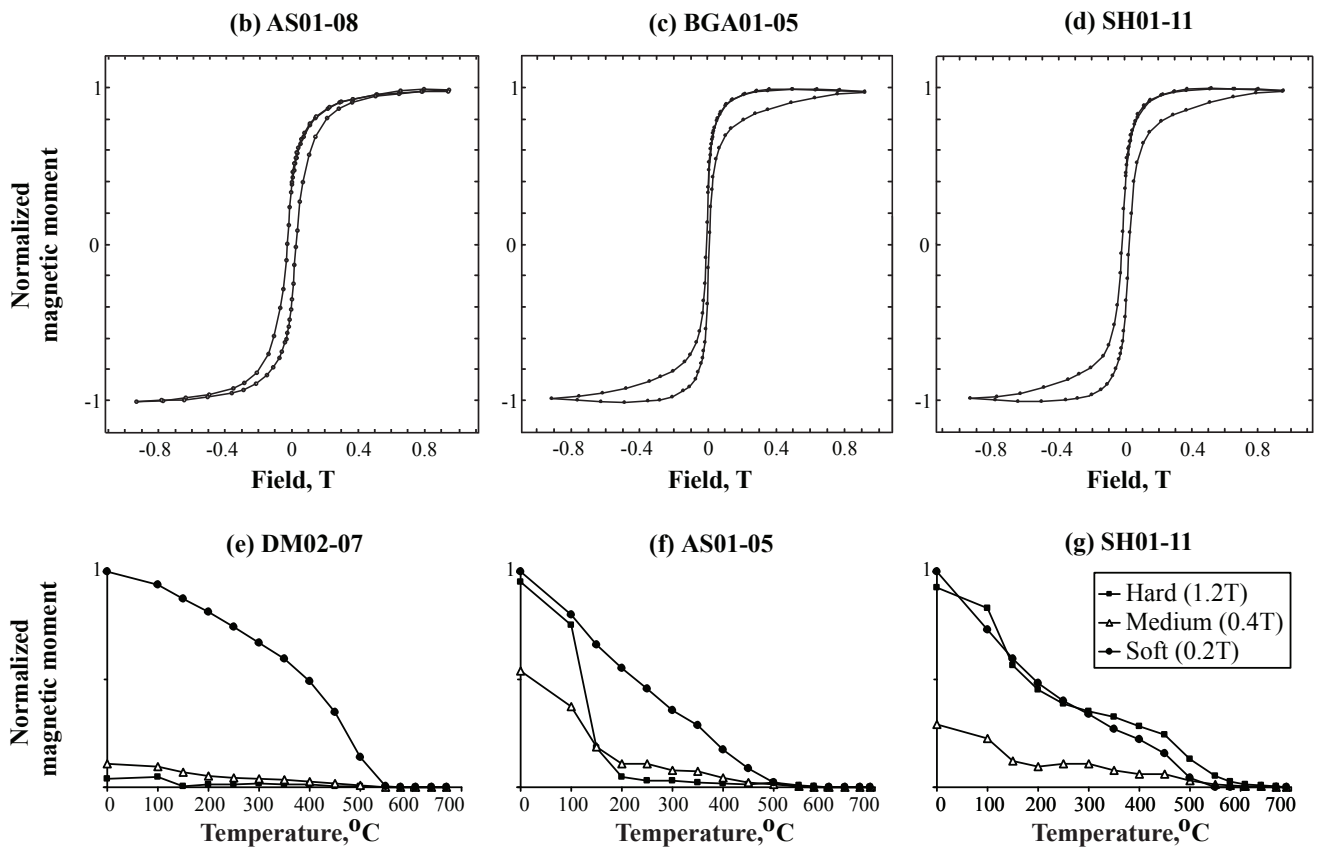
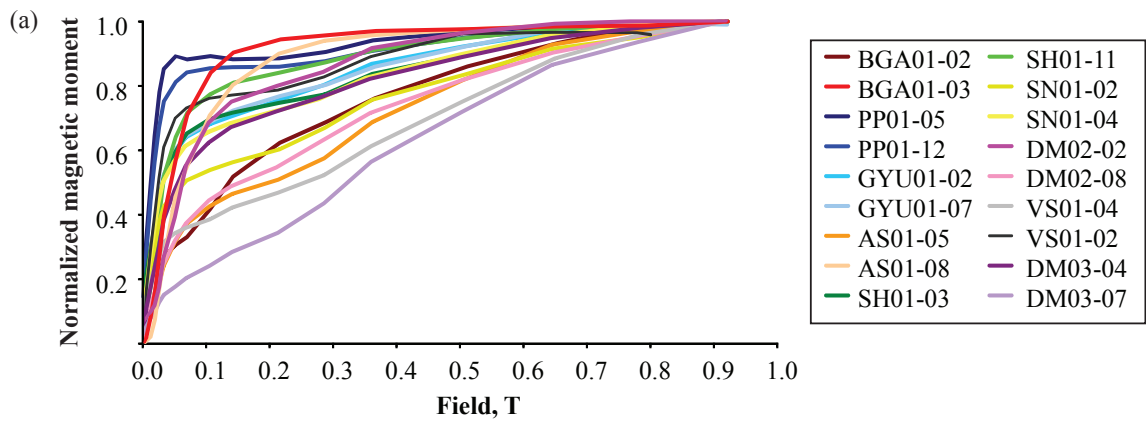


Figure 5



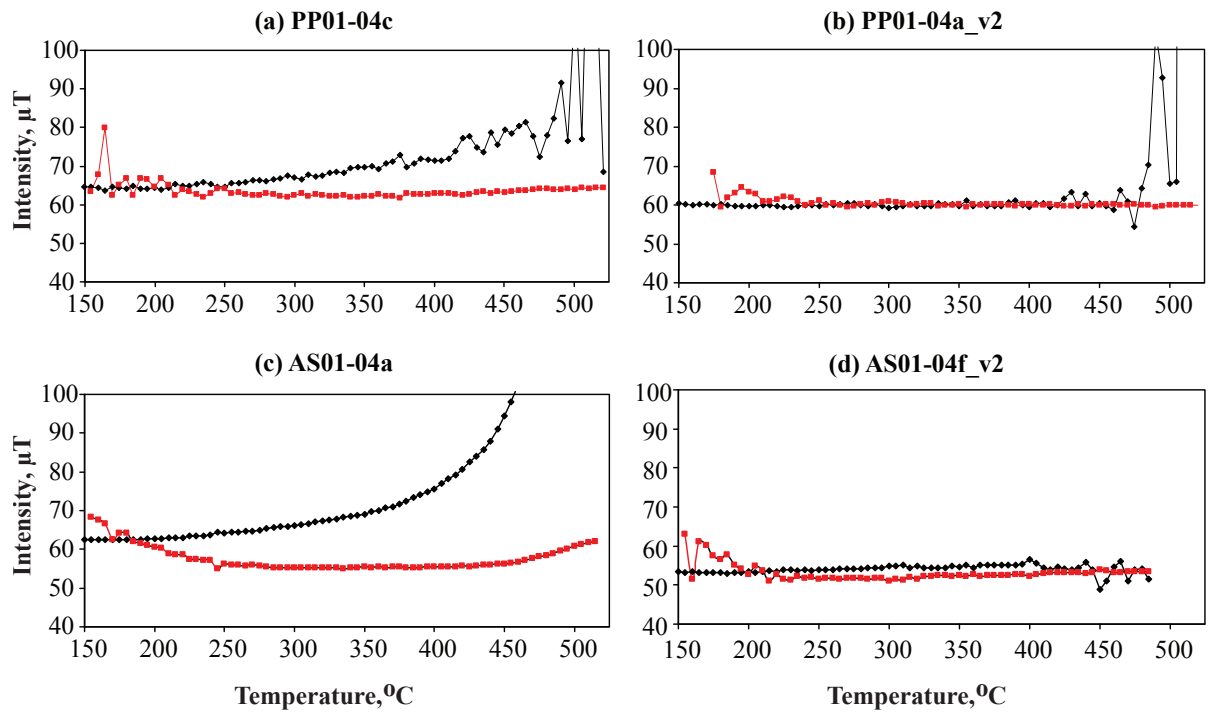


Figure 6

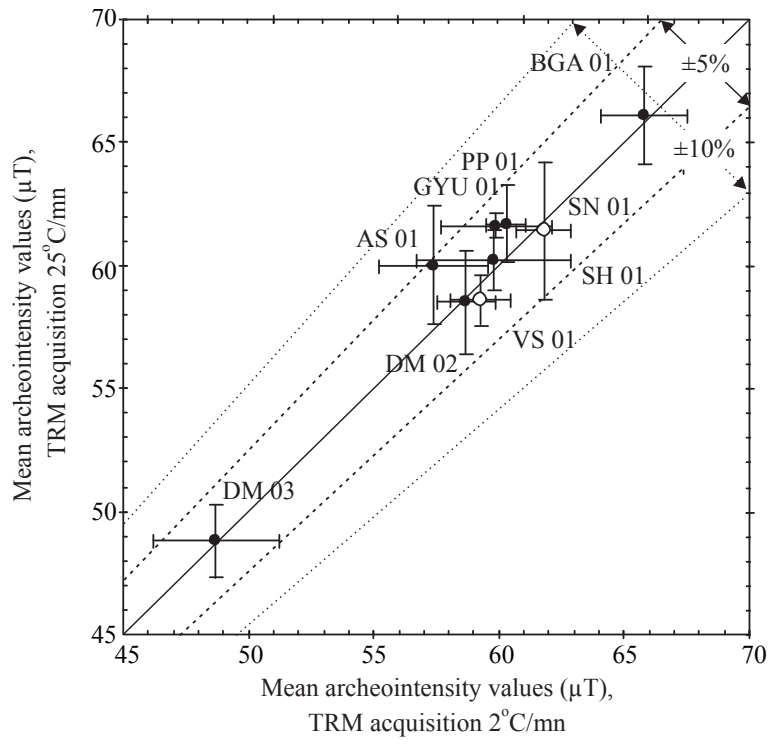


Figure 7

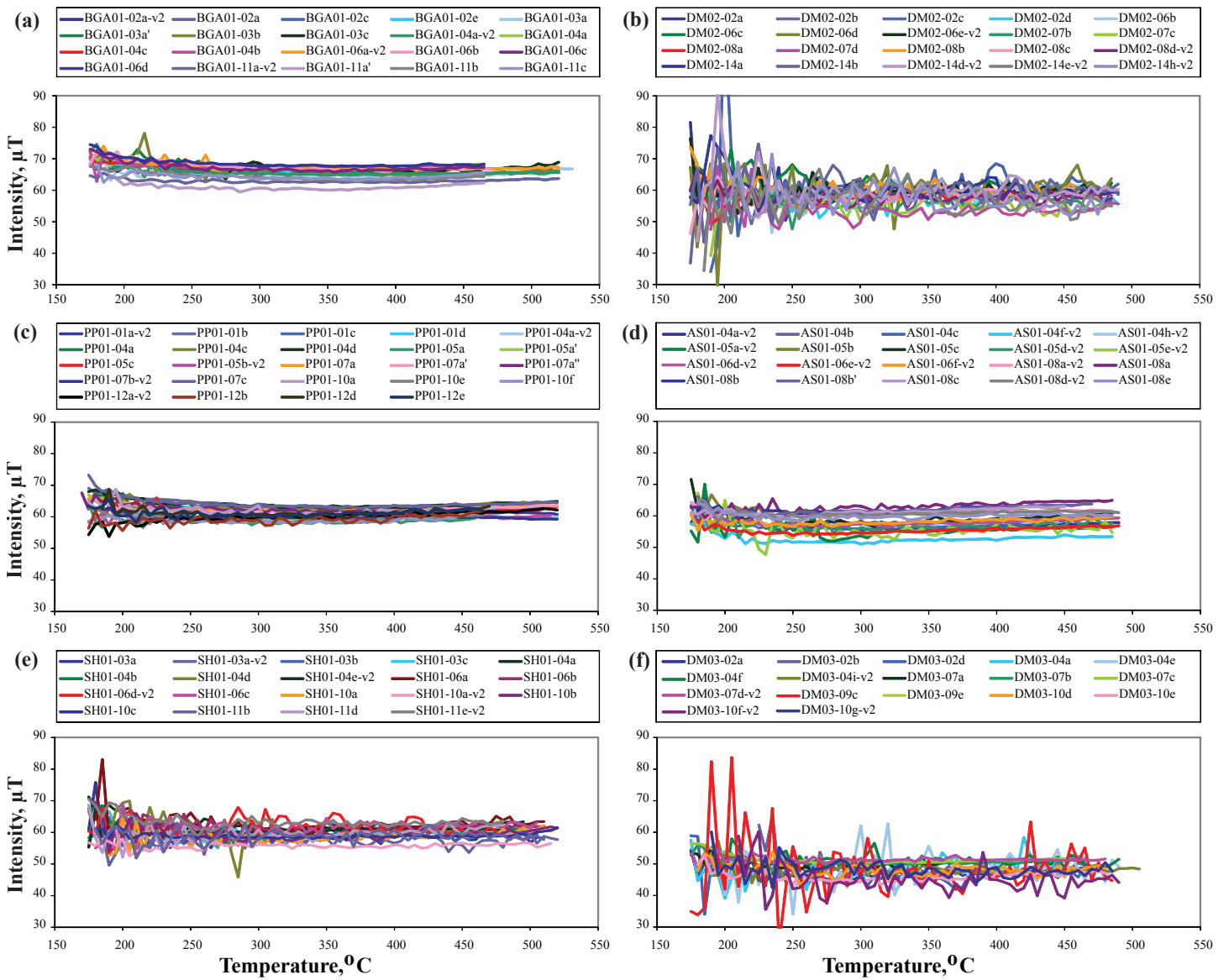


Figure 8

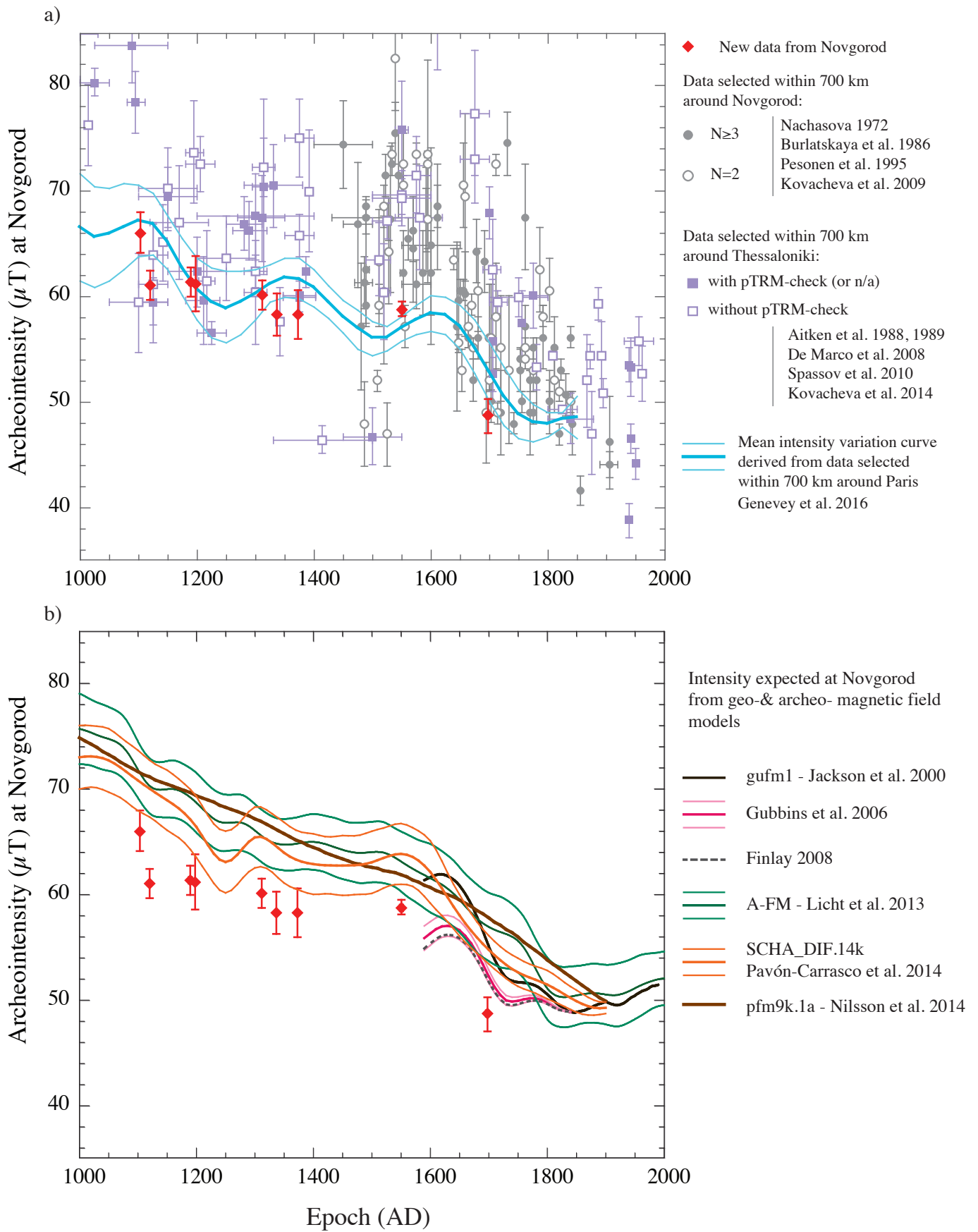


Figure 9

Table 1

Archeomagnetic group	Lat (°N)	Long (°E)	Site	Age (AD)	N fragments	n specimens	F <sub>mean</sub> ±σF (μT)
BGA01	58.49	31.30	Church of the Annunciation in the Gorodishche	1103	5	21	66.1±1.9
GYU01	58.49	31.28	Monastery church of St. Georgi	1119	3	11	61.1±1.4
PP01	58.51	31.26	Church to the Holy Apostels Peter and Paul in Silnishche	1185 - 1192	6	25	61.4±1.4
SN01	58.50	31.31	Transfiguration church on Nereditsa hill	1198	4	17	61.2±2.6
SH01	58.48	31.30	Holy Virgin Protection church of Shilov Monastery	1310	5	20	60.1±1.4
DM02	58.56	31.30	Church of the Holy Resurrection on the Derevyanitsa river	1335	5	21	58.3±2.0
AS01	58.50	31.33	Church of St Andrew the Holy Fool on Sitka	1371	4	20	58.3±2.3
VS01	58.58	31.23	Cathedral of Our Lady of Vladimir of Syrkov Monastery	1548 - 1554	3	13	58.8±0.7
DM03	58.56	31.30	Church of the Holy Resurrection on the Derevyanitsa river	1695 - 1697	5	17	48.7±1.6

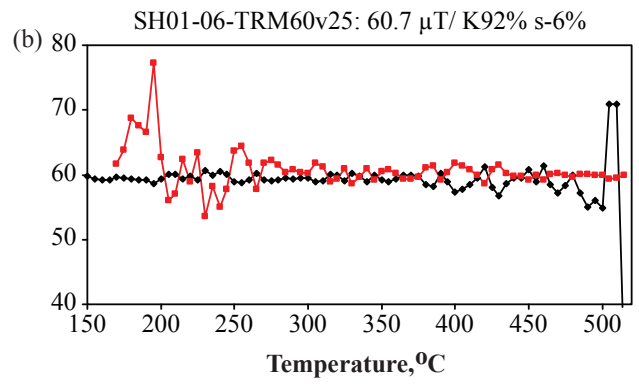
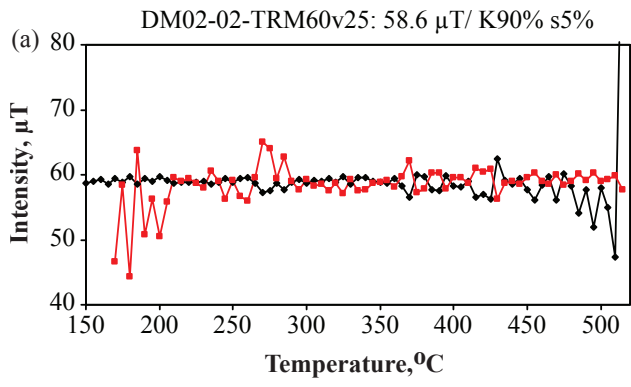


Figure S1

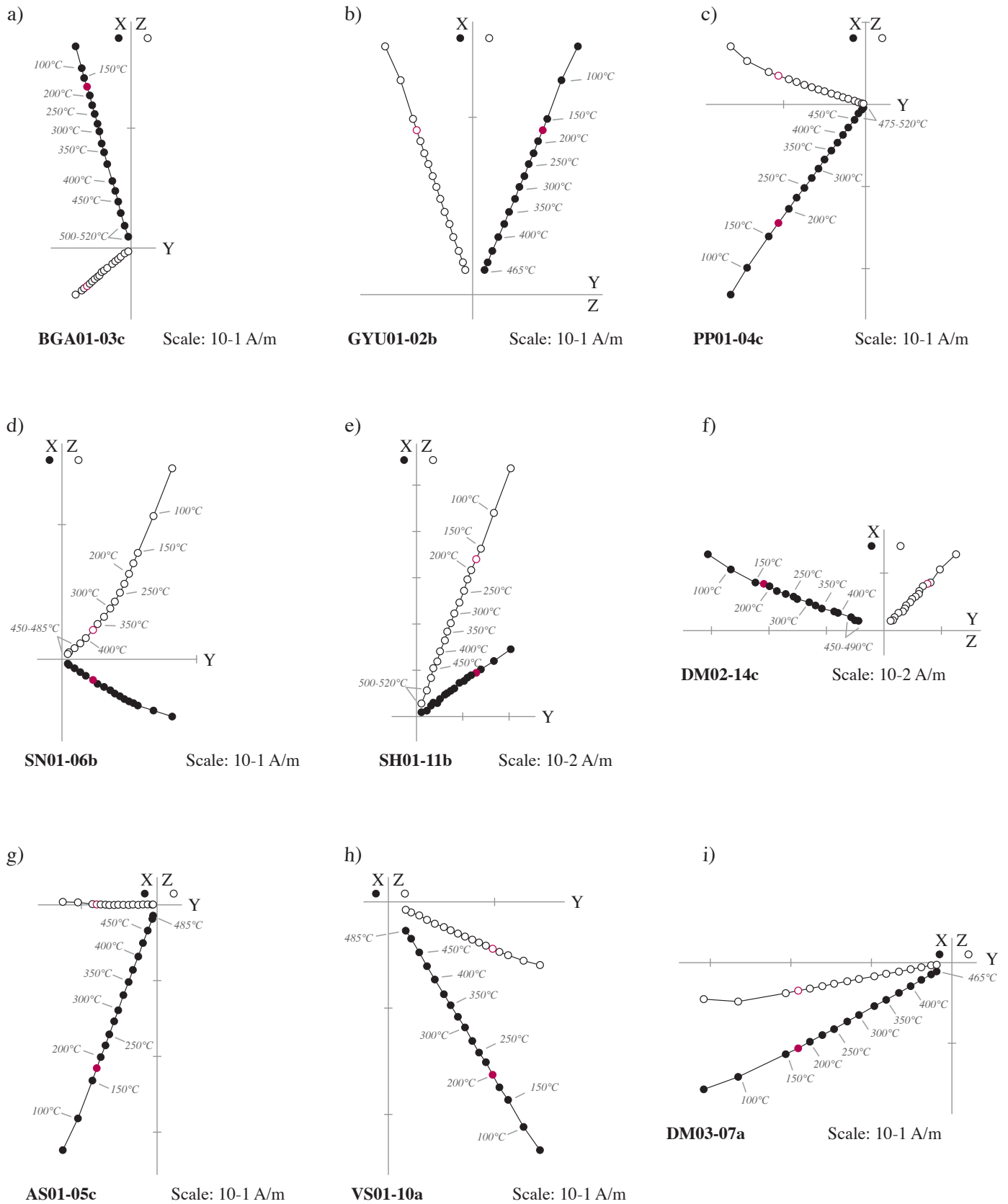


Figure S2

Fragment	Specimen	T <sub>min</sub> - T <sub>max</sub> (°C)	F <sub>Lab</sub>	Cooling rate, (°C/mn)	NRM T1 (T1') (%)	Slope R' (%)	F <sub>Triaxe</sub> (μT)	F <sub>Triaxe</sub> mean value per fragment ±σF (μT)
1	2	3	4	5	6	7	8	9

***BGA01, Novgorod, The Church of the Annunciation in the Gorodishche, [1103] AD, (12/12/5)***

BGA01-02	BGA01-02a	175–465	65	25	83	-8	65.8	66.0±0.4
	BGA01-02c	175–515	65	25	92	-2	65.5	
	BGA01-02e	175–465	65	25	83	-6	66.1	
	BGA01-02a-v2	180–520	65	2	96	-6	66.5	
BGA01-03	BGA01-03a	180–530	65	25	95	-2	65.2	66.4±1.0
	BGA01-03a'	205–465	65	25	65	-5	67.3	
	BGA01-03c	180–520	65	25	89	-2	67.1	
	BGA01-03b-v2	210–520	65	2	95	-5	66.0	
BGA01-04	BGA01-04b	175–465	65	25	87	-2	68.0	67.3±0.9
	BGA01-04c	175–465	65	25	86	-2	67.5	
	BGA01-04d	175–465	65	25	90	-2	67.6	
	BGA01-04a-v2	175–520	65	2	95	-5	65.9	
BGA01-06	BGA01-06b	175–470	65	25	84	-6	67.6	67.8±0.6
	BGA01-06c	175–465	65	25	84	-5	67.3	
	BGA01-06d	175–465	65	25	84	-5	68.6	
	BGA01-06a-v2	180–520	65	2	96	-5	67.7	
BGA01-11	BGA01-11a	205–445	65	25	66	-4	61.8	62.9±1.5
	BGA01-11a'	195–465	65	25	79	0	60.9	
	BGA01-11b	175–465	65	25	79	-5	64.4	
	BGA01-11c	180–465	65	25	74	-1	64.3	
	BGA01-11a-v2	175–520	65	2	95	-1	63.0	

***GYU01, Novgorod, The monastery Church of St. Georgi, [1119] AD, (7/7/3)***

GYU01-01	GYU01-02b	180–465	65	25	78	-3	61.6	59.7±1.7
	GYU01-02c	215–485	65	25	55	8	60.5	
	GYU01-02a-v2	175–485	65	2	89	4	58.0	
	GYU01-02e-v2	180–465	65	2	69	3	58.5	
GYU01-04	GYU01-04a-v2	180–485	65	2	91	1	62.0	62.4±0.4
	GYU01-04d-v2	180–485	65	2	91	-1	62.4	
	GYU01-04f-v2	175–480	60	2	91	-2	62.7	
GYU01-07	GYU01-07a	215–485	65	25	56	5	61.5	61.4±1.7
	GYU01-07b	200–485	65	25	51	2	61.5	
	GYU01-07c	175–485	65	25	67	-4	63.3	
	GYU01-07f-v2	175–480	60	2	87	0	59.1	



1	2	3	4	5	6	7	8	9
---	---	---	---	---	---	---	---	---

**PP01, Novgorod, The Church to the Holy Apostels Peter and Paul in Silnishche, [1185 – 1192] AD, (12/10/6)**

PP01-01	PP01-01b	175–510	60	25	95	-5	64.3	62.7±1.1
	PP01-01c	180–510	60	25	96	-3	62.1	
	PP01-01d	180–510	60	25	96	-1	62.6	
	PP01-01a-v2	200–520	60	2	97	-4	61.9	
PP01-04	PP01-04a	175–440	60	25	80	-4	63.0	62.8±1.6
	PP01-04c	175–520	60	25	96	-1	63.7	
	PP01-04d	175–520	60	25	96	-3	64.0	
	PP01-04a-v2	195–520	60	2	98	-3	60.4	
PP01-05	PP01-05c	185–520	60	25	92	0	61.4	60.0±1.1
	PP01-05a	175–460	60	25	76	-2	58.8	
	PP01-05a'	175–445	60	25	70	-5	60.1	
	PP01-05b-v2	175–515	60	2	93	1	59.7	
PP01-07	PP01-07a	175–520	60	25	97	-2	62.7	62.3±1.5
	PP01-07a'	180–520	60	25	97	1	62.2	
	PP01-07a''	170–465	60	25	88	-6	62.6	
	PP01-07c	175–520	60	25	97	-5	64.2	
	PP01-07b-v2	175–520	60	2	97	-3	60.0	
PP01-10	PP01-10a	175–460	60	25	85	-4	61.8	59.9±1.3
	PP01-10e	175–465	60	25	84	-2	59.4	
	PP01-10f	175–445	60	25	81	0	58.7	
	PP01-10a-v2	170–505	60	2	91	-1	59.6	
PP01-12	PP01-12b	175–465	60	25	78	5	59.1	60.4±1.1
	PP01-12d	185–465	60	25	75	0	61.4	
	PP01-12e	175–465	60	25	76	1	61.2	
	PP01-12a-v2	175–520	60	2	93	9	60.0	

**SN01, Novgorod, The Transfiguration church on Nereditsa hill, [1198] AD, (11/9/4)**

SN01-02	SN01-02a	190–485	60	25	91	1	61.0	60.8±0.8
	SN01-02a'	200–465	60	25	79	-4	59.6	
	SN01-02b	205–465	60	25	81	2	61.2	
	SN01-02c	200–465	60	25	82	-3	61.6	
	SN01-02d-v2	195–480	60	2	91	-3	60.7	
SN01-04	SN01-04a	175–485	60	25	91	-3	57.5	57.9±2.6
	SN01-04b	180–485	60	25	74	0	55.6	
	SN01-04c	175–480	60	25	90	-7	60.7	
SN01-06	SN01-06b	375–485	60	25	79	3	62.6	64.2±1.8
	SN01-06d	350–485	60	25	78	3	65.9	
	SN01-06e	375–485	60	25	75	2	65.6	
	SN01-06f-v2	375–485	60	2	73	5	62.8	

1	2	3	4	5	6	7	8	9
SN01-09	SN01-09a	395–485	60	25	86	-1	62.4	62.0±1.1
	SN01-09b	395–485	60	25	87	3	61.6	
	SN01-09c	395–485	60	25	87	4	63.4	
	SN01-09d	385–485	60	25	88	6	62.2	
	SN01-09e	380–485	60	25	89	4	60.3	

***SH01, Novgorod, Holy Virgin Protection church of Shilov monastery, [1310] AD, (8/8/5)***

SH01-03	SH01-03a	175–510	60	25	75	-1	59.1	59.2±1.1
	SH01-03b	175–505	60	25	73	2	59.1	
	SH01-03c	175–505	60	25	74	-1	60.6	
	SH01-03a-v2	180–510	60	2	74	-3	57.8	
SH01-04	SH01-04a	175–495	60	25	95	-6	62.6	61.1±1.1
	SH01-04b	175–495	60	25	93	-5	60.2	
	SH01-04d	175–480	60	25	81	-1	61.2	
	SH01-04e-v2	175–480	60	2	86	3	60.5	
SH01-06	SH01-06a	180–510	60	25	77	-1	62.4	61.8±0.5
	SH01-06b	205–510	60	25	74	0	61.3	
	SH01-06c	180–505	60	25	75	5	61.5	
	SH01-06d-v2	175–475	60	2	55	-1	61.8	
SH01-10	SH01-10a	190–520	60	25	86	5	58.7	58.2±1.7
	SH01-10b	180–520	60	25	94	-2	59.6	
	SH01-10c	180–520	60	25	86	0	58.9	
	SH01-10a-v2	175–515	60	2	92	1	55.7	
SH01-11	SH01-11b	180–520	60	25	86	1	58.8	60.3±2.1
	SH01-11c	180–520	60	25	85	-6	59.3	
	SH01-11d	175–480	60	25	53	4	59.6	
	SH01-11e-v2	175–480	60	2	53	-4	63.4	

***DM02, Novgorod, Church of the Holy Resurrection by the river Derevyanitsa, [1335]AD, (10/9/5)***

DM02-02	DM02-02a	175–485	65	25	61	5	58.9	58.9±1.2
	DM02-02b	175–485	65	25	70	6	58.1	
	DM02-02c	190–490	65	25	64	2	60.5	
	DM02-02d	175–490	65	25	69	-1	57.9	
DM02-06	DM02-06b	225–490	65	25	73	6	59.5	60.4±0.9
	DM02-06c	175–485	65	25	72	-6	61.7	
	DM02-06d	175–485	65	25	69	8	60.2	
	DM02-06e-v2	175–480	60	2	64	-3	60.1	
DM02-07	DM02-07b	195–485	65	25	64	-1	56.2	55.0±1.3
	DM02-07c	190–485	65	25	63	-2	55.0	
	DM02-07d	190–490	65	25	62	-3	53.7	
DM02-08	DM02-08a	175–485	65	25	66	6	57.7	58.4±1.1
	DM02-08b	175–485	65	25	66	-7	60.1	
	DM02-08c	175–485	65	25	64	5	57.9	
	DM02-08d-v2	175–485	60	2	65	-5	58.0	

1	2	3	4	5	6	7	8	9
DM02-14	DM02-14a	175–490	65	25	59	-5	60.2	58.9±1.7
	DM02-14b	175–490	65	25	70	0	59.6	
	DM02-14c	185–490	65	25	69	-2	59.7	
	DM02-14d	180–490	65	2	57	-6	60.3	
	DM02-14e	185–485	60	2	66	1	56.4	
	DM02-14h	200–480	60	2	64	-7	57.2	

*AS01, Novgorod, The church of St Andrew the Holy Fool on Sitka, [1371] AD, (11/6/4)*

AS01-04	AS01-04b	175–470	65	25	78	1	58.1	56.4±2.2
	AS01-04c	175–450	65	25	60	-1	56.9	
	AS01-04a-v2	175–490	65	2	82	0	56.7	
	AS01-04f-v2	175–485	60	2	91	-1	52.7	
	AS01-04h-v2	175–445	60	2	68	-2	57.8	
AS01-05	AS01-05b	180–445	65	25	74	-2	61.1	57.7±2.4
	AS01-05c	175–485	65	25	90	-1	59.2	
	AS01-05a-v2	175–485	65	2	89	-2	55.7	
	AS01-05d-v2	180–485	60	2	82	-2	57.0	
	AS01-05e-v2	180–485	60	2	76	-2	55.7	
AS01-06	AS01-06d-v2	180–490	60	2	86	2	58.0	57.2±1.6
	AS01-06e-v2	180–490	60	2	90	3	55.4	
	AS01-06f-v2	175–485	60	2	89	3	58.2	
AS01-08	AS01-08a	175–485	65	25	72	7	62.9	61.6±1.1
	AS01-08b	180–450	65	25	84	3	61.9	
	AS01-08b'	180–470	65	25	81	4	62.0	
	AS01-08b''	175–485	65	25	88	4	63.3	
	AS01-08c	175–450	65	25	80	5	61.3	
	AS01-08d-v2	180–490	60	2	90	1	60.8	
	AS01-08e-v2	180–485	60	2	88	-1	60.0	
	AS01-08a-v2	175–485	65	2	84	2	60.9	

*VS01, Novgorod, Cathedral of Our Lady of Vladimir in Syrkov Monastery, [1548 – 1554] AD, (11/5/3)*

VS01-02	VS01-02a	200–465	50	25	58	-9	58.5	58.5±2.2
	VS01-02b	180–465	50	25	66	6	55.4	
	VS01-02d	195–465	60	25	58	-8	59.5	
	VS01-02a-v2	175–510	50	2	90	-8	60.5	
VS01-04	VS01-04b	175–485	50	25	82	0	61.0	58.3±1.6
	VS01-04c	175–465	60	25	66	3	57.0	
	VS01-04d	175–485	60	25	62	-5	58.5	
	VS01-04f	175–465	60	25	68	1	57.0	
	VS01-04a-v2	175–510	50	2	86	-6	58.1	
VS01-10	VS01-10a	195–485	50	25	77	-3	59.5	59.7±0.2
	VS01-10b	200–465	60	25	63	-5	59.6	
	VS01-10c	180–465	60	25	70	-8	60.0	
	VS01-10d	200–465	60	25	61	-2	59.6	

1	2	3	4	5	6	7	8	9
<i>DM03, Novgorod, Church of the Holy Resurrection by the river Derevyanitsa, [1695 – 1697] AD, (11/8/5)</i>								
DM03-02	DM03-02a	175–465	50	25	70	-2	47.2	47.6±1.3
	DM03-02b	225–465	50	25	62	-9	49.1	
	DM03-02d	175–470	50	25	61	-4	46.5	
DM03-04	DM03-04a	175–465	50	25	60	10	48.6	49.1±1.0
	DM03-04e	195–490	50	25	57	2	49.1	
	DM03-04f	190–490	50	25	55	-1	50.5	
	DM03-04i-v2	180–505	50	2	51	-4	48.2	
DM03-07	DM03-07a	175–465	50	25	86	1	50.2	50.9±0.6
	DM03-07b	175–465	50	25	84	-1	50.6	
	DM03-07c	175–465	50	25	84	-4	51.4	
	DM03-07d	175–480	50	2	90	-1	51.4	
DM03-09	DM03-09c	175–485	50	25	53	-3	48.2	49.2±1.0
	DM03-09e	175–480	50	25	56	-3	50.1	
DM03-10	DM03-10d	180–480	50	25	53	-2	47.9	46.7±1.6
	DM03-10e	180–480	50	25	56	0	46.1	
	DM03-10f-v2	210–490	50	2	54	-9	44.7	
	DM03-10g-v2	190–485	50	2	60	-7	48.2	